

THEORETICAL INVESTIGATION OF COMPLEXES OF URANYL(II), VANADYL(II) AND ZIRCONYL(II) WITH VITAMIN B13 AS CANDIDATE COMPOUNDS AS ANTI-NONALCOHOLIC FATTY LIVER DISEASE AND *DIABETES MELLITUS* TARGETS

Amnah Mohammed Alsuhaibani¹, Sonam Shakya² and Moamen S. Refat^{3*}

¹Department of Physical Sport Science, College of Sport Sciences & Physical Activity, Princess Nourah bint Abdulrahman University, P.O. Box 84428, Riyadh 11671, Saudi Arabia

²Department of Chemistry, Faculty of Science, Aligarh Muslim University, Aligarh 202002, India

³Department of Chemistry, College of Science, Taif University, P.O. Box 11099, Taif 21944, Saudi Arabia

(Received June 10, 2024; Revised August 2, 2024; Accepted August 2, 2024)

ABSTRACT. Density functional theory (DFT) calculations were carried out utilizing the B3LYP functional in conjunction with the 6-311G++ and LanL2DZ basis sets to explore the molecular properties and geometries of Vitamin (Vit) B13 and its complexes with Uranyl (II), Vanadyl (II), and Zirconyl (II). The optimized structures, molecular electrostatic potential maps, key molecular properties, and HOMO-LUMO energy gaps of these compounds were systematically examined to gain insights into their electronic characteristics and stability. Bioactivity screenings of the synthesized complexes were performed using molecular docking studies to investigate their interactions with diabetes mellitus (DM) target proteins, specifically the Insulin Receptor (IR) (PDB ID: 1IR3) and the peroxisome proliferator-activated receptor- γ (PPAR γ) (PDB ID: 3K8S). These receptors play pivotal roles in the PPAR and AMP-activated protein kinase (AMPK) signaling pathways, which are essential for protecting against nonalcoholic fatty liver disease (NAFLD). The docking results highlighted the binding affinities and potential bioactivity of Vit B13 and its metal complexes, suggesting their promise as therapeutic agents against DM and NAFLD. This comprehensive computational study provides valuable insights into the molecular interactions and electronic properties of these compounds, paving the way for further experimental validation and potential pharmaceutical applications.

KEY WORDS: Vitamin B13, Metal complexes, *Diabetes mellitus*, Molecular docking, DFT

INTRODUCTION

We performed computational calculations using Density Functional Theory (DFT) at the B3LYP/6-311G++ and LanL2DZ level of theory [1]. This study encompassed the analysis of optimized geometries, molecular electrostatic potential maps, and the electronic energy gaps between the Highest Occupied Molecular Orbital (HOMO) and the Lowest Unoccupied Molecular Orbital (LUMO) for Vitamin (Vit) B13 and its synthesized complexes (UO₂(II)Vit B13, VO(II)Vit B13, and ZrO(II)Vit B13) [2]. Additionally, important parameters such as structural, chemical, and spectroscopic properties were thoroughly investigated and corroborated. We conducted a comprehensive theoretical study to examine the interactions between Vit B13 and its synthesized complexes (UO₂(II)Vit B13, VO(II)Vit B13, and ZrO(II)Vit B13) with two critical receptors: (i) The Insulin Receptor (IR) (PDB ID: 1IR3), which is activated by insulin, Insulin-like Growth Factor 1 (IGF-1), and Insulin Growth Factor 2 (IGF-II). Disruptions in the production or response to these factors are significant contributors to Diabetes Mellitus (DM) [3]. (ii) The Peroxisome Proliferator-Activated Receptor- γ (PPAR γ) (PDB ID: 3K8S), which plays a pivotal role in regulating the PPAR and AMP-activated protein kinase (AMPK) signaling pathways, crucial for protecting against nonalcoholic fatty liver disease (NAFLD) [4].

*Corresponding authors. E-mail: moamen@tu.edu.sa; msrefat@yahoo.com

This work is licensed under the Creative Commons Attribution 4.0 International License

Using the molecular docking method with AutoDock Vina software, we compared the binding affinities and interactions of Vit B13 and its complexes with these receptors. Our analysis encompassed several critical parameters: binding energy, interpolated charge, solvent-accessible surface area (SAS), ionizability, hydrophobic interactions, hydrogen bonding, and aromatic interactions at the binding sites. This comprehensive approach allowed us to gain an in-depth understanding of the molecular interactions and potential therapeutic efficacy of these compounds [5-9].

EXPERIMENTAL

Density functional theory (DFT)

It is worth mentioning in this research that vitamin B13 compounds with vanadyl, zirconyl, and uranyl salts were previously prepared in aqueous media with reaction ratios of 1 to 2 (metal salt: vitamin B13). These compounds were characterized using spectroscopic and thermal analyzes and concluded the results led to the development of proposed forms for these compounds and their previous published [2]. We employed the Gaussian 09RevD.01 software package [10] for our density functional theory (DFT) calculations. These calculations aimed to obtain optimized molecular geometries and investigate electronic transitions in Vit B13 and its synthesized complexes (UO₂(II)Vit B13, VO(II)Vit B13, and ZrO(II)Vit B13). The geometry optimization was performed using the B3LYP/6-311G++ basis set, incorporating Becke's three-parameter hybrid exchange function combined with the Pople basis set and the Los Alamos Effective Core Potentials (LanL2DZ) basis set for the U, V, and Zr atom [11]. Our study extended to several key properties, including molecular electrostatic potential (MEP) maps and the analysis of the frontier molecular orbitals (FMOs), specifically the highest occupied molecular orbital (HOMO) and the lowest unoccupied molecular orbital (LUMO). These properties were crucial for evaluating the electronic characteristics and chemical stability of Vit B13 and its complexes [12].

Furthermore, we calculated infrared frequencies, which were consistently positive, confirming that the optimized geometries correspond to minima on the potential energy surface. By examining the vibrational modes, we accurately assigned the bands observed in the FT-IR spectra of both the parent compound and its complexes. We also extended our theoretical investigation to structure-based molecular properties in the gas phase using the same computational methods. For visualization of the molecular structures and properties, we utilized ChemCraft 1.5 software [13]. This comprehensive theoretical analysis provides valuable insights into the electronic structure and stability of Vit B13 and its complexes, contributing to a deeper understanding of their potential applications in various fields.

Molecular docking

The initial molecular structures of Vit B13 and its synthesized complexes (UO₂(II)Vit B13, VO(II)Vit B13, and ZrO(II)Vit B13), optimized through density functional theory (DFT) calculations, served as the starting geometries for our study. These structures were converted to PDBQT format using OpenBabelGUI software version 2.4.1 [14, 15], which is available at http://openbabel.org/wiki/Main_Page. For the receptors, Insulin Receptor (IR) (PDB ID: 1IR3) and Peroxisome Proliferator-Activated Receptor- γ (PPAR γ) (PDB ID: 3K8S), structural data were retrieved from the RCSB Protein Data Bank [16].

The receptor structures were prepared for docking by removing the native ligands and other heteroatoms, including water molecules, using BIOVIA Discovery Studio Visualizer (v19.1.0.18287). To ensure accurate docking, polar hydrogen atoms were added, and Kollman charges were assigned using Autodock Tools [17]. Partial charges were assigned following the Gasteiger method. The docking of Vit B13 and its complexes with the receptors was conducted using Autodock Vina [18]. The resulting docked poses were analyzed to evaluate the interactions,

with detailed scrutiny performed using Discovery Studio (DS) Visualizer (<https://www.3ds.com/products-services/biovia/>). The docking simulations were executed on a computer with the following specifications: Intel(R) Core(TM) i5-4200U CPU @ 1.60 GHz, 2.10 GHz, 2.30 GHz, 64-bit architecture. This rigorous computational approach allowed us to gain insights into the binding interactions and potential efficacy of Vit B13 and its complexes as therapeutic agents. The detailed analysis of the docking poses provided valuable information on the molecular interactions at the binding sites of the target receptors [19].

RESULTS AND DISCUSSIONS

Density functional theory calculations

We employed the B3LYP functional combined with the 6-311G++ and LanL2DZ basis sets to achieve optimized structures for Vit B13 and its synthesized complexes: $\text{UO}_2(\text{II})\text{Vit B13}$, $\text{VO}(\text{II})\text{Vit B13}$, and $\text{ZrO}(\text{II})\text{Vit B13}$. The Self-Consistent Field (SCF) energy calculations revealed that the minimum energy for Vit B13 was -595.257938 atomic units (a.u.) after 16 optimization steps. For the complexes $\text{UO}_2(\text{II})\text{Vit B13}$, $\text{VO}(\text{II})\text{Vit B13}$, and $\text{ZrO}(\text{II})\text{Vit B13}$, the minimum SCF energies were determined to be -2134.017716 a.u., -1632.252663 a.u., and -1607.426095 a.u., respectively. The optimized geometries, along with the detailed atomic coordinates and strain-free lattice constants, can be seen in Figure 1. These optimized parameters provide a robust foundation for subsequent analyses, ensuring the accuracy and reliability of our computational results. This meticulous optimization process is critical for understanding the electronic structure and potential reactivity of these complexes. The electrostatic potential strengths for Vit B13 and its synthesized complexes ($\text{UO}_2(\text{II})\text{Vit B13}$, $\text{VO}(\text{II})\text{Vit B13}$, and $\text{ZrO}(\text{II})\text{Vit B13}$) are illustrated in the Molecular Electrostatic Potential (MEP) maps, shown in Figure 2.

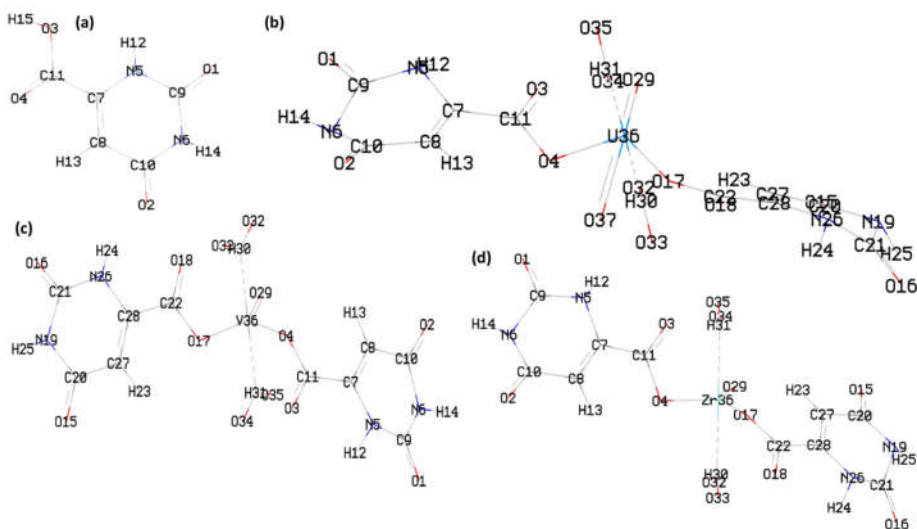


Figure 1. Optimized structure of (a) Vit B13, (b) $\text{UO}_2(\text{II})\text{Vit B13}$ complex, (c) $\text{VO}(\text{II})\text{Vit B13}$ complex, and (d) $\text{ZrO}(\text{II})\text{Vit B13}$ complex with Mulliken atom numbering scheme.

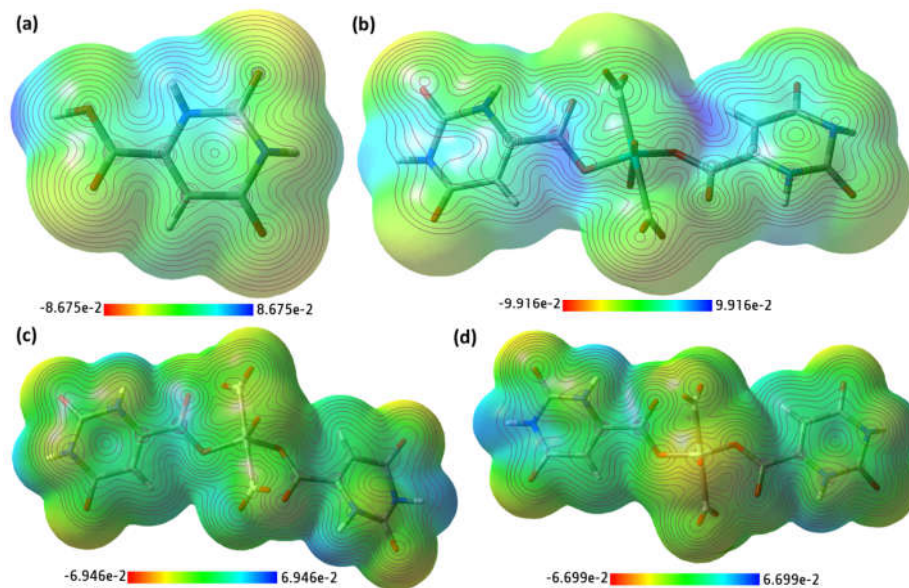


Figure 2. MEP surface map obtained from optimized structure of (a) Vit B13, (b) $\text{UO}_2(\text{II})\text{Vit B13}$ complex, (c) $\text{VO}(\text{II})\text{Vit B13}$ complex, and (d) $\text{ZrO}(\text{II})\text{Vit B13}$ complex with respective color scales.

These maps use a color scale where electropositive regions are represented in blue and electronegative regions in red, highlighting the preferential binding sites for electrophilic and nucleophilic interactions on the molecules [20]. The MEP surface maps are presented on a color scale ranging from deep red to deep blue, corresponding to the following ranges: $-0.08675\text{e-}2$ to $+0.08647\text{e-}2$ for Vit B13, $-0.09916\text{e-}2$ to $+0.09916\text{e-}2$ for the $\text{UO}_2(\text{II})\text{Vit B13}$ complex, $-0.06946\text{e-}2$ to $+0.06946\text{e-}2$ for the $\text{VO}(\text{II})\text{Vit B13}$ complex, and $-0.06699\text{e-}2$ to $+0.06699\text{e-}2$ for the $\text{ZrO}(\text{II})\text{Vit B13}$ complex. These ranges provide a clear visualization of the electrostatic potential distribution and indicate the reactive sites for potential interactions, as shown in Figure 2. By analyzing these MEP maps, we can identify the regions on each molecule that are most likely to engage in electrophilic or nucleophilic interactions, providing insights into their chemical behavior and potential applications [21].

We conducted an in-depth investigation of the infrared spectra of Vit B13 and its synthesized complexes ($\text{UO}_2(\text{II})\text{Vit B13}$, $\text{VO}(\text{II})\text{Vit B13}$, and $\text{ZrO}(\text{II})\text{Vit B13}$) in the gas phase using density functional theory (DFT) at the B3LYP/LanL2DZ level of theory. This computational approach was employed to complement and corroborate experimental findings. The simulated IR spectra were scaled by a factor of 0.9001, as illustrated in Figure 3. Several key vibrational signals observed in the experimental FTIR spectra were found to align well with those in the simulated infrared spectra. This correlation was confirmed by analyzing the animated vibrational modes [22]. It is important to note that some deviations between the simulated and experimental data are anticipated due to the inherent simplifications and anharmonicity within the basis set used in the DFT calculations. Consequently, a scaling factor was applied to the simulated vibrational frequencies to achieve better agreement with the experimental results. These findings demonstrate that the DFT-based simulated spectra effectively replicate the experimental observations, thereby validating the theoretical model and providing deeper insights into the vibrational characteristics of Vit B13 and its complexes [23].

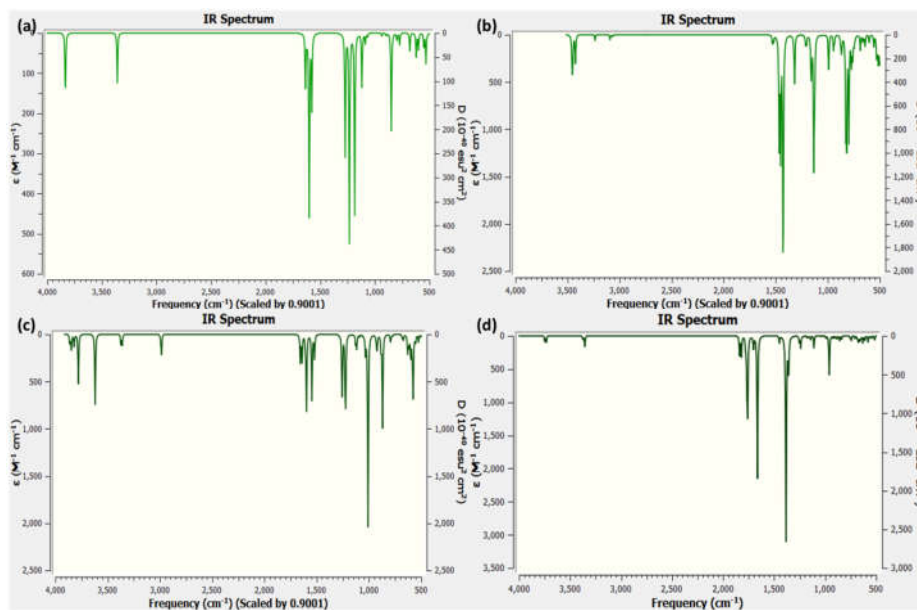


Figure 3. Simulated (DFT) IR spectra of (a) Vit B13, (b) $\text{UO}_2(\text{II})\text{Vit B13}$ complex, (c) $\text{VO}(\text{II})\text{Vit B13}$ complex, and (d) $\text{ZrO}(\text{II})\text{Vit B13}$ complex.

We investigated the electronic transitions of Vit B13 and its synthesized complexes ($\text{UO}_2(\text{II})\text{Vit B13}$, $\text{VO}(\text{II})\text{Vit B13}$, and $\text{ZrO}(\text{II})\text{Vit B13}$) in the gas phase using Time-Dependent Density Functional Theory (TD-DFT). The TD-DFT calculations revealed maximum absorption bands at wavelengths of 288 nm for Vit B13, 319 nm for the $\text{UO}_2(\text{II})\text{Vit B13}$ complex, 301 nm for the $\text{VO}(\text{II})\text{Vit B13}$ complex, and 298 nm for the $\text{ZrO}(\text{II})\text{Vit B13}$ complex [24]. These results are presented in Figure 4, which also illustrates the spatial arrangements of the Highest Occupied Molecular Orbital (HOMO) and the Lowest Unoccupied Molecular Orbital (LUMO), as well as the HOMO-LUMO energy gaps for each compound. The HOMO-LUMO energy gap (ΔE) was found to be 4.3084 eV for Vit B13, 3.8866 eV for the $\text{UO}_2(\text{II})\text{Vit B13}$ complex, 4.1191 eV for the $\text{VO}(\text{II})\text{Vit B13}$ complex, and 4.1605 eV for the $\text{ZrO}(\text{II})\text{Vit B13}$ complex [25]. These energy gaps provide insights into the chemical stability of the molecules, with smaller energy gaps indicating higher chemical reactivity, lower kinetic stability, and a softer nature. Conversely, larger energy gaps suggest higher stability and lower reactivity. Based on the energy gaps, the stability order of the complexes is as follows: $\text{UO}_2(\text{II})\text{Vit B13}$ complex > $\text{VO}(\text{II})\text{Vit B13}$ complex > $\text{ZrO}(\text{II})\text{Vit B13}$ complex > Vit B13. Table 1 provides a summary of various molecular parameters derived from the gas-phase analysis, including HOMO-LUMO properties and optimized geometries. These comprehensive data underscore the significant electronic characteristics and stability profiles of Vit B13 and its synthesized complexes, contributing valuable insights into their potential applications and reactivity profiles [26].

Molecular docking studies

We conducted comprehensive molecular docking studies to investigate the interactions between Vit B13 and its synthesized complexes ($\text{UO}_2(\text{II})\text{Vit B13}$, $\text{VO}(\text{II})\text{Vit B13}$, and $\text{ZrO}(\text{II})\text{Vit B13}$) with two critical receptors: the Insulin Receptor (IR), PDB ID: 1IR3, associated with *Diabetes*

mellitus (DM), and the peroxisome proliferator-activated receptor- γ (PPAR γ), PDB ID: 3K8S, linked with nonalcoholic fatty liver disease (NAFLD). Our goal was to identify the most favorable docking poses and evaluate the relative binding efficiencies of Vit B13 and its complexes. The results of our docking studies revealed significant insights into the binding affinities of these compounds. The UO₂(II)Vit B13 complex demonstrated a higher potential binding energy compared to Vit B13 and the other synthesized complexes for both receptors. Specifically, the UO₂(II)Vit B13 complex exhibited the highest docking energy value when interacting with the IR receptor, with a potential binding energy of -9.9 kcal/mol. This indicates a stronger interaction between the UO₂(II)Vit B13 complex and the IR receptor compared to the other complexes. Table 2 presents a detailed comparison of the docking data, including the potential binding energies for Vit B13 and its synthesized complexes with both receptors. The most favorable docking poses for Vit B13 and its complexes with the IR and PPAR γ receptors are illustrated in Figure 5. Additionally, the molecular docking interactions are depicted in both 3D and 2D representations for the IR receptor in Figure 6, and for the PPAR γ receptor in Figure 7. These findings highlight the superior binding affinity of the UO₂(II)Vit B13 complex, suggesting its potential as a more effective therapeutic agent for conditions related to these receptors. Our comprehensive docking analysis provides valuable insights into the molecular interactions and stability of these complexes, paving the way for further experimental validation and potential pharmaceutical applications [27]. As shown in Figure 6, Vit B13 with IR reveals the amino acid residues, including Glu1115 and Phe1144 forming hydrogen bond interactions. Additionally, Thr1145 and Ser1270 forming unfavorable Donor-Donor and Acceptor-Acceptor interaction, respectively, are also present [28, 29]. On the other hand UO₂(II)Vit B13 complex with IR for hydrogen bond with Ser1006, Met1079, Glu1043, Asp1150, Lys1030, and Glu1047 including carbon-hydrogen bond with Gly1082 and Gly1005 (Figure 6). Similarly, molecular docking of Vit B13 with PPAR γ reveals the amino acid residues, Ser342 and Ile262 forming hydrogen bond interactions (Figure 7).

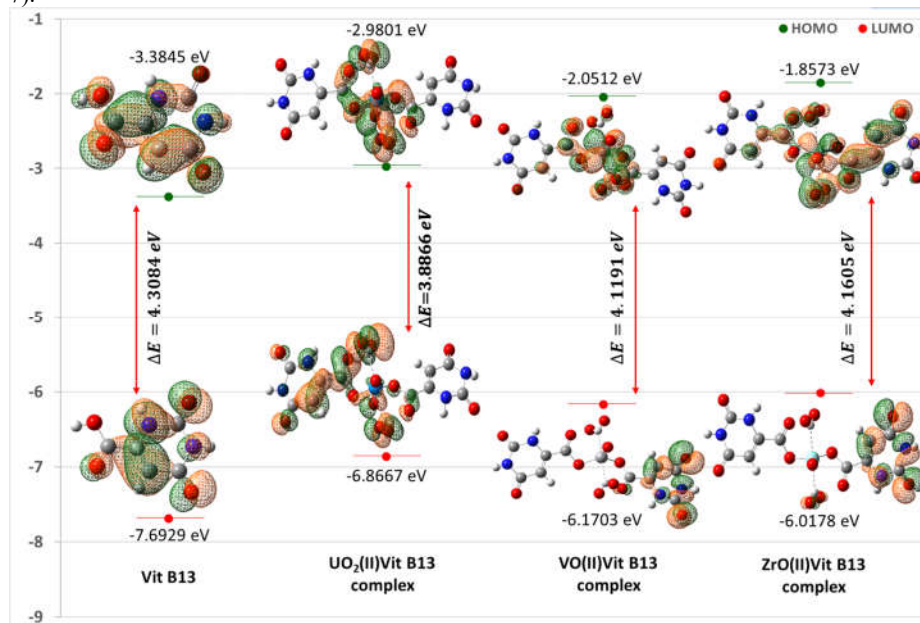


Figure 4. Spatial plot of HOMO and LUMO with their energy gap for Vit B13, UO₂(II)Vit B13 complex, VO(II)Vit B13 complex, and ZrO(II)Vit B13 complex.

Table 1. Various other theoretical molecular parameters of Vit B13, UO₂(II)Vit B13 complex, VO(II)Vit B13 complex, and ZrO(II)Vit B13 complex.

Parameters	RB3LYP/ lanL2DZ			
	Vit B13	UO ₂ (II)Vit B13complex	VO(II)Vit B13complex	ZrO(II)Vit B13complex
Minimum SCF energy (a.u.)	-595.257938	-2134.017716	-1632.252663	-1607.426095
Polarizability (α) (a.u.)	50.504173	311.389706	193.666219	284.546308
Dipole Moment (Debye)	2.446221	1.519423	2.701496	3.582718
Zero point vibrational energy (kcal/mol)	61.53578	131.52684	135.23466	135.12899
Total thermal energy (kcal/mol)	66.482	144.839	147.377	145.329
Electronic spatial extent (a.u.)	1822.4368	17580.9576	17312.1560	17324.9202
Frontier MO energies (eV)				
LUMO	-3.3845	-2.9801	-2.0512	-1.8573
HOMO	-7.6929	-6.8667	-6.1703	-6.0178
Gap (HOMO – LUMO)	4.3084	3.8866	4.1191	4.1605

Table 2. The interactions of Vit B13 and synthesized complex docked with two receptors [IR (PDB ID: 1IR3) and PPARγ (PDB ID: 3K8S)].

S.No.	Ligand+Receptor	Binding free energy (kcal/mol)	Interactions	
			H-Bond	Others
1	Vit B13+ IR	-5.5	Glu1115 and Phe1144	Thr1145 and Ser1270 (Unfavorable Donor-Donor and Acceptor-Acceptor)
2	UO ₂ (II)Vit B13complex+ IR	-9.9	Ser1006, Met1079, Glu1043, Asp1150, Lys1030, and Glu1047	Gly1082 and Gly1005 (Carbon hydrogen bond)
3	VO(II)Vit B13complex + IR	-8.1	Glu1043, Lys1030, Arg1136, and Asn1137	Gly1005 (Carbon Hydrogen Bond)
4	ZRO(II)Vit B13complex + IR	-7.9	Glu1043, Lys1030, Arg1136, and Asn	Gly1005 (Carbon Hydrogen Bond)
5	Vit B13+ PPARγ	-5.9	Ser342 and Ile262	-
6	UO ₂ (II)Vit B13complex+ PPARγ	-8.8	Glu295, Arg288, Glu343, Ser342, and Leu228	Arg288 and Glu343 (Carbon Hydrogen Bond)
7	VO(II)Vit B13complex + PPARγ	-8.3	Ser289, Tyr327, Gln286, Lys367, His449, and Cys285	His449 (Carbon Hydrogen Bond)
8	ZRO(II)Vit B13complex + PPARγ	-6.8	Asp381, Glu378, Arg234, and Lys230	-

On the other hand UO₂(II)Vit B13complex with PPARγ for hydrogen bond with Glu295, Arg288, Glu343, Ser342, and Leu228 including carbon hydrogen bond with Arg288 and Glu343 (Fig. 7). These findings suggest that the synthesized UO₂(II)Vit B13 complex exhibits more efficient binding with both IR and PPARγ receptors, especially with IR as UO₂(II)Vit B13 complex forms multiple hydrogen bonds and carbon-hydrogen bonds with key amino acid residues in both receptors, enhancing its stability and binding efficiency. These interactions

suggest that the $\text{UO}_2(\text{II})\text{Vit B13}$ complex could potentially be more effective as a therapeutic agent for conditions associated with these receptors.

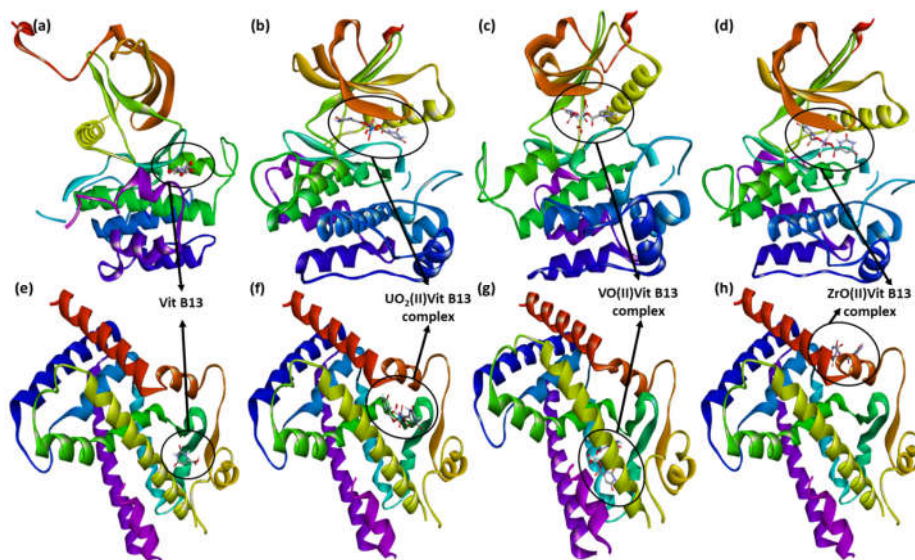


Figure 5. Best docked pose showing a helical model of (a,b,c,d) IR (PDB ID: 1IR3) docked with Vit B13, $\text{UO}_2(\text{II})\text{Vit B13}$ complex, $\text{VO}(\text{II})\text{Vit B13}$ complex, and $\text{ZrO}(\text{II})\text{Vit B13}$ complex, respectively, and (e, f, g, h) $\text{PPAR}\gamma$ (PDB ID: 3K8S) docked with Vit B13, $\text{UO}_2(\text{II})\text{Vit B13}$ complex, $\text{VO}(\text{II})\text{Vit B13}$ complex, and $\text{ZrO}(\text{II})\text{Vit B13}$ complex, respectively.

Surface interaction study by Discovery Studio (DS) software

We performed an in-depth analysis of the molecular docking results using Discovery Studio (DS) software, which provided comprehensive visualization tools for examining the interaction surfaces between the ligands and receptor binding sites. This sophisticated software enabled us to generate detailed graphical representations of the interaction sites, showcasing various physicochemical properties [30]. Figure 8 presents a series of graphical illustrations that highlight the key interaction features at the binding sites. These include aromatic interactions, hydrogen bonding, hydrophobic interactions, interpolated charge, ionizability, and solvent-accessible surface (SAS) surfaces.

The topographical features of aromatic surfaces hold significant importance in molecular modeling, drug design, and structural analysis owing to their pivotal role in identifying putative binding sites, elucidating molecular recognition mechanisms, and forecasting intermolecular interactions. Particularly, in investigations concerning interactions mediated by aromatic rings, which exert substantial influence in diverse biological and chemical contexts, the delineation of aromatic surface characteristics assumes paramount significance [31]. In the present study, visualization of the aromatic face and edge surfaces (depicted as orange and blue, respectively, as illustrated in Figure 8a) provides insights into their spatial arrangement and electrostatic properties, thereby enriching our comprehension of molecular interactions. A depiction of hydrogen bond surface figures (as illustrated in Figure 8b) provides a visual representation of the intricate hydrogen bonding interactions inherent within a molecular framework. This graphical

representation employs a color-coded scheme to highlight amino acid residues participating in hydrogen bonding, distinguishing hydrogen atom acceptor sites in green and donor sites in pink. The interconnection of these sites through lines or dashed lines serves to delineate the hydrogen bonds, with emphasis placed on delineating the donor and acceptor roles through color differentiation.

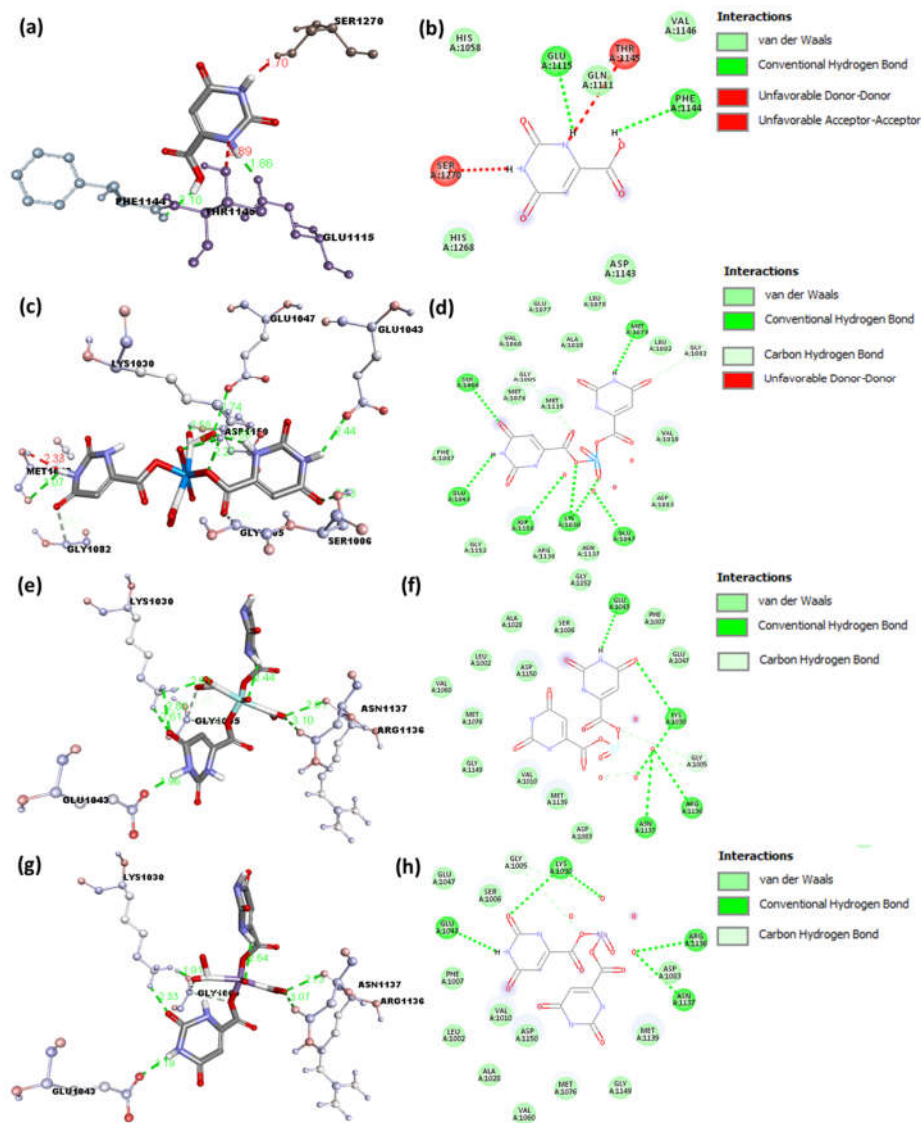


Figure 6. (a, c, e, g) 3D representation and (b, d, f, g) 2D representation of interactions for IR (PDB ID: 1IR3) docked with (a, b) Vit B13, (c, d) $\text{UO}_2(\text{II})\text{Vit B13}$ complex, (e, f) $\text{VO}(\text{II})\text{Vit B13}$ complex, and (g, h) $\text{ZrO}(\text{II})\text{Vit B13}$ complex, respectively.

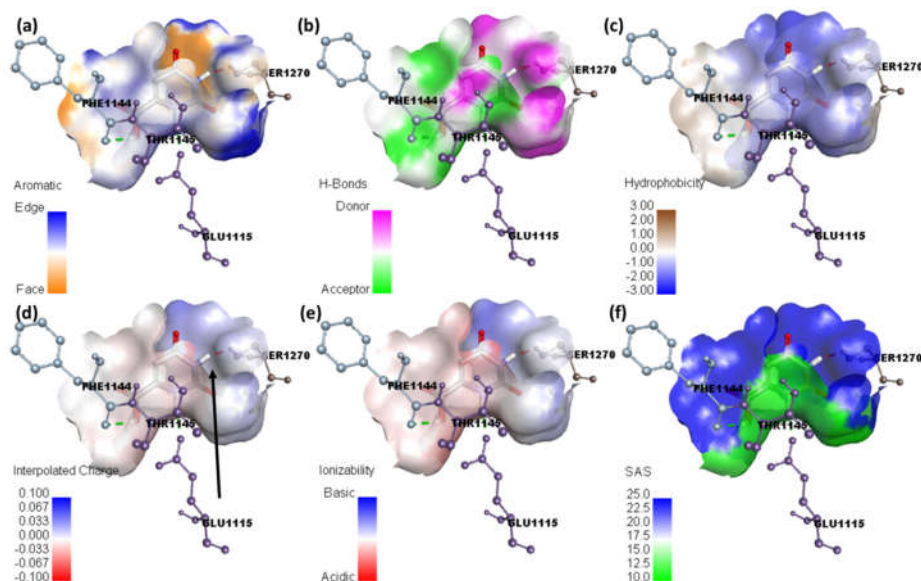


Figure 8. Representation of (a) aromatic surface, (b) hydrogen binding surface, (c) hydrophobic surface, (d) Interpolated charge, (e) ionizability surface, and (f) solvent accessible surface; between IR (PDB ID: 1IR3) and Vit B13.

Through this graphical depiction, the figure succinctly elucidates the hydrogen bond topology, accentuating the specific amino acid residues engaged in these crucial interactions. Hydrophobicity surface figures (as depicted in Figure 8c) offer a visual portrayal of the hydrophobic domains inherent within a molecular framework. Conventionally, hydrophobic regions are depicted in varying shades of blue, while hydrophilic regions maintain neutral coloring or display contrasting hues. Such visual representations serve to elucidate the interaction dynamics between molecules and water, wherein hydrophobic regions exhibit a repulsion towards aqueous environments. The discernment of hydrophilic features surrounding the ligand by means of hydrophobicity surface analysis confirms the presence of complementary hydrophilic interactions within the receptor-ligand interface. This is confirmed through hydrophobicity surface analysis, revealing hydrophilic regions surrounding the ligand. These interactions enhance binding stability and specificity by facilitating favorable water-mediated contacts, crucial for the overall binding affinity and molecular recognition between the receptor and ligand. Interpolated charge calculation entails the determination of partial atomic charges distributed across a molecule, thereby augmenting the precision of molecular modeling [32]. This methodological approach holds significance in predicting electrostatic interactions, pivotal for comprehending binding affinities and refining drug design strategies through meticulous examination of molecular properties and interactions (see Figure 8d). Ionization surface figures (depicted in Figure 8e) serve as visual representations delineating the acidic and basic characteristics of a molecular surface. In this graphical depiction, regions exhibiting basic properties are denoted in shades of blue, while those manifesting acidic tendencies are portrayed in hues of red. Such representations aid in discerning the electrostatic profile of molecular surfaces, offering insights into potential charge-based interactions [33]. Solvent accessible surface (SAS) figures (illustrated in Figure 8f) provide a visual depiction of the surface area of a receptor accessible to solvent molecules, a crucial parameter in elucidating molecular interactions. In this visualization, areas characterized by

limited solvent accessibility are depicted in green to indicate regions that are less prone to solvent penetration due to their hydrophobic nature or structural hindrance. These regions typically involve parts of the molecule that are buried within the protein structure or are shielded by other molecular components, reducing the likelihood of interaction with solvent molecules. This limited accessibility can influence the molecule's stability and interaction dynamics, making it an important factor in understanding molecular interactions and drug design [34]. Conversely, regions with heightened accessibility are highlighted in blue, with an emphasis on polar regions. This graphical representation facilitates the identification of molecular sites poised for interaction with the surrounding solvent environment, thereby enriching our understanding of solvation effects [35, 36].

CONCLUSION

Theoretical data acquired via Density Functional Theory (DFT) calculations have played a pivotal role in elucidating the molecular geometry of the compounds under investigation. Examination of the band gap energies of Vitamin (Vit) B13 and its synthesized complexes (UO₂(II)-Vit B13 complex, VO(II)-VitB13 complex, and ZrO(II)-Vit B13 complex), reveals a notable trend wherein the UO₂(II)Vit B13 complex demonstrates highest stability compared to the others. These molecular parameters, derived through DFT analysis, furnish valuable insights that can guide and inform future research endeavors in this domain. Molecular docking studies have revealed that the synthesized UO₂(II)Vit B13 complex exhibits enhanced interaction efficiency with both the Insulin Receptor (IR), associated with Diabetes Mellitus, and the peroxisome proliferator-activated receptor- γ (PPAR γ), linked with nonalcoholic fatty liver disease. Significantly, the UO₂(II)Vit B13 complex demonstrates the highest binding affinity for IR, as evidenced by its superior binding energy values. Additionally, surface binding studies corroborate these findings, confirming that the UO₂(II)Vit B13 complex engages more robustly with these receptors compared to other complexes. This enhanced interaction underscores its potential therapeutic efficacy.

ACKNOWLEDGMENT

The authors extend their appreciation to Taif University, Saudi Arabia, for supporting this work through project number (TU-DSPP-2024-06).

FUNDING

This research was funded by Taif University, Saudi Arabia, Project No. (TU-DSPP-2024-06).

REFERENCES

1. Al-Hazmi, G.H.; Hassanien, A.M.; Atta, A.A.; Refat, M.S.; Saad, H.A.; Shakya, S.; Adam, A.M.A. Supramolecular charge-transfer complex generated by the interaction between tin(II) 2,3-naphthalocyanine as a donor with DDQ as an acceptor: Spectroscopic studies in solution state and theoretical calculations. *J. Mol. Liq.* **2022**, *362*, 119757.
2. Refat, M.S. Complexes of uranyl(II), vanadyl(II) and zirconyl(II) with orotic acid "vitamin B13": Synthesis, spectroscopic, thermal studies and antibacterial activity. *J. Mol. Struc.* **2007**, *842*, 24-37.
3. Singh, P.; Singh, V.K.; Singh, A.K. Molecular docking analysis of candidate compounds derived from medicinal plants with type 2 diabetes mellitus targets. *Bioinformation* **2019**, *15*, 179-188.

- Tang, Z.; Li, L.; Xia, Z. Exploring anti-nonalcoholic fatty liver disease mechanism of *Gardeniae fructus* by network pharmacology, molecular docking, and experiment validation. *ACS Omega* **2022**, *7*, 25521-25531.
- Khan, M.S.; Kamal, S.; Zulkiflain, M.; Khalid, M.; Khan, S.; Shahid, M.; Ahmad, M. Tailored coordination chemistry: A novel Zn(II)-fluorescent coordination material for highly selective and sensitive detection of Hg²⁺ ions in aqueous environments. *J. Mol. Liq.* **2024**, *405*, 125019.
- Khan, M.S.; Li, Y.; Yang, L.; Yan, Z.C.; Li, D.S.; Qiu, J.; Xu, X.; Yang, H.Y. Improving capacitive deionization performance through tailored iodine-loaded ZIF-8 composites. *Desalination*. **2024**, *579*, 117486.
- Khan, M.S.; Ansari, M.A.H.; Khalid, M.; Shahid, M.; Ahmad, M. Synthesis, characterization, single-crystal X-ray study and sensing properties of a designed dinuclear Cu(II) system. *Inorg. Nano-Met. Chem.* **2023**, DOI: 10.1080/24701556.2023.2188454.
- Khan, M.S.; Khalid, M.; Ahmad, M.S.; Kamal, S.; Shahid, M.; Ahmad, M. Effect of structural variation on enzymatic activity in tetranuclear (Cu₄) clusters with defective cubane core. *J. Biomol. Struct. Dyn.* **2022**, *40*, 9067-9080.
- Khan, M.S.; Hayat, M.U.; Khanam, M.; Saeed, H.; Owais, M.; Khalid, M.; Shahid, M.; Ahmad, M. Role of biologically important imidazole moiety on the antimicrobial and anticancer activity of Fe(III) and Mn(II) complexes. *J. Biomol. Struct. Dyn.* **2021**, *39*, 4037-4050.
- Frisch, M.J.; Trucks, G.W.; Schlegel, H.B.; Scuseria, G.E.; Robb, M.A.; Cheeseman, J.R.; Scalmani, G.; Barone, V.; Petersson, G.A.; Nakatsuji, H.; Li, X.; Caricato, M.; Marenich, A.V.; Bloino, J.; Janesko, B.G.; Gomperts, R.; Mennucci, B.; Hratchian, H.P.; Ortiz, J.V.; Izmaylov, A.F.; Sonnenberg, J.L.; Williams-Young, D.; Ding, F.; Lipparini, F.; Egidi, F.; Goings, J.; Peng, B.; Petrone, A.; Henderson, T.; Ranasinghe, D.; Zakrzewski, V.G.; Gao, J.; Rega, N.; Zheng, G.; Liang, W.; Hada, M.; Ehara, M.; Toyota, K.; Fukuda, R.; Hasegawa, J.; Ishida, M.; Nakajima, T.; Honda, Y.; Kitao, O.; Nakai, H.; Vreven, T.; Throssell, K.; Montgomery, J.A., Jr.; Peralta, J.E.; Ogliaro, F.; Bearpark, M.J.; Heyd, J.J.; Brothers, E.N.; Kudin, K.N.; Staroverov, V.N.; Keith, T.A.; Kobayashi, R.; Normand, J.; Raghavachari, K.; Rendell, A.P.; Burant, J.C.; Iyengar, S.S.; Tomasi, J.; Cossi, M.; Millam, J.M.; Klene, M.; Adamo, C.; Cammi, R.; Ochterski, J. W.; Martin, R.L.; Morokuma, K.; Farkas, O.; Foresman, J.B.; Fox, D.J. *Gaussian 09*, Gaussian, Inc.: Wallingford CT; **2009**.
- Salih, R.H.H.; Hasan, A.H.; Hussein, A.J.; Samad, M.K.; Shakya, S.; Jamalis, J.; Hawaiz, F.E.; Pratama, M.R.F. One-pot synthesis, molecular docking, ADMET, and DFT studies of novel pyrazolines as promising SARS-CoV-2 main protease inhibitors. *Res Chem. Intermed.* **2022**, *48*, 4729-4751.
- Hariharan, P.C.; Pople, J.A. The effect of d-functions on molecular orbital energies for hydrocarbons. *Chem. Phys. Lett.* **1972**, *16*, 217-219.
- Zhurko G.A.; Zhurko D.A. Chemcraft - graphical program for visualization of quantum chemistry computations. Ivanovo, Russia, Academic version 1.5, **2004**.
- O'Boyle, N.M.; Banck, M.; James, C.A.; Morley, C.; Vandermeersch, T.; Hutchison, G.R. Open Babel: An open chemical toolbox. *J. Cheminf.* **2011**, *3*, 1-14.
- Dallakyan, S. PyRx-python prescription v. 0.8. *The Scripps Research Institute*, 2008. **2010**.
- Chu, C.-H.; Li, K.-M.; Lin, S.W.; Chang, M.D.T.; Jiang, T.Y.; Sun, Y.J. Crystal structures of starch binding domain from *Rhizopus oryzae* glucoamylase in complex with isomaltooligosaccharide: Insights into polysaccharide binding mechanism of CBM21 family. *Proteins: Struct. Funct. Bioinf.* **2014**, *82*, 1079-1085.
- Rehman, M.T.; AlAjmi, M.F.; Hussain, A. Natural compounds as inhibitors of SARS-CoV-2 main protease (3CLpro): A molecular docking and simulation approach to combat COVID-19. *Curr. Pharm. Des.* **2021**, *27*, 3577-3589.

18. Trott, O.; Olson, A.J. AutoDock Vina: Improving the speed and accuracy of docking with a new scoring function, efficient optimization, and multithreading. *J. Comput. Chem.* **2010**, *31*, 455-461.
19. Shakya, S.; Khan, I.M.; Shakya, B.; Siddique, Y.H.; Varshney, H.; Jyoti, S. Protective effect of the newly synthesized and characterized charge transfer (CT) complex against arecoline induced toxicity in third-instar larvae of transgenic *Drosophila melanogaster* (hsp70-lacZ) Bg 9: Experimental and theoretical mechanistic insights. *J. Mater. Chem. B.* **2023**, *11*, 1262-1278.
20. Shakya, S.; Khan, I.M.; Ahmad, M. Charge transfer complex based real-time colorimetric chemosensor for rapid recognition of dinitrobenzene and discriminative detection of Fe²⁺ ions in aqueous media and human hemoglobin. *J. Photochem. Photobiol. A Chem.* **2020**, *392*, 112402.
21. Islam, M.R.; Shakya, S.; Selim, A.; Alam, M.S.; Ali, M. Solvatochromic absorbance and fluorescence probe behavior within ionic liquid+ γ -butyrolactone mixture. *J. Chem. Eng. Data* **2019**, *64*, 4169-4180.
22. Yu, W.; He, X.; Vanommeslaeghe, K.; MacKerell, A.D., Jr. Extension of the CHARMM general force field to sulfonylcontaining compounds and its utility in biomolecular simulations. *J. Comput. Chem.* **2012**, *33*, 2451-2468.
23. Abraham, M.J.; Murtola, T.; Schulz, R.; Páll, S.; Smith, J.C.; Hess, B.; Lindahl, E. GROMACS: High performance molecular simulations through multi-level parallelism from laptops to supercomputers. *SoftwareX.* **2015**, *1*, 19-25.
24. Murugavel, S.; Ravikumar, C.; Jaabil, G.; Alagusundaram, P. Synthesis, crystal structure analysis, spectral investigations (NMR, FT-IR, UV), DFT calculations, ADMET studies, molecular docking and anticancer activity of 2-(1-benzyl-5-methyl-1H-1,2,3-triazol-4-yl)-4-(2-chlorophenyl)-6-methoxypyridine—a novel potent human topoisomerase II α inhibitor. *J. Mol. Struct.* **2019**, *1176*, 729-742.
25. Khan, I.M.; Shakya, S. Exploring colorimetric real-time sensing behavior of a newly designed CT complex toward nitrobenzene and Co²⁺: Spectrophotometric, DFT/BarCS-DFT, and mechanistic insights. *ACS Omega* **2019**, *4*, 9983-9995.
26. Refat, M.S.; Gaber, A.; Althobaiti, Y.S.; Alyami, H.; Alsanie, W.F.; Shakya, S.; Adam, A.M.A.; Kobeasy, M.I.; Asla, K.A. Spectroscopic and molecular docking studies of Cu(II), Ni(II), Co(II), and Mn(II) complexes with anticonvulsant therapeutic agent gabapentin. *Molecules* **2022**, *27*, 4311.
27. Akram, M.; Lal, H.; Shakya, S.; Kabir-ud-Din. Multispectroscopic and computational analysis insight into the interaction of cationic diester-bonded gemini surfactants with serine protease α -chymotrypsin. *ACS Omega* **2020**, *5*, 3624-3637.
28. Khan, I.M.; Shakya, S.; Islam, M.; Khan, S.; Najnin, H. Synthesis and spectrophotometric studies of CT complex between 1, 2-dimethylimidazole and picric acid in different polar solvents: exploring antimicrobial activities and molecular (DNA) docking. *Phys. Chem. Liq.* **2021**, *59*, 753-769.
29. Khan, I.M.; Islam, M.; Shakya, S.; Alam, N.; Imtiaz, S.; Islam, M.R. Synthesis, spectroscopic characterization, antimicrobial activity, molecular docking and DFT studies of proton transfer (H-bonded) complex of 8-aminoquinoline (donor) with chloranilic acid (acceptor). *J. Biomol. Struct. Dyn.* **2022**, *40*, 12194-12208.
30. Krivák, R.; Jendele, L.; Hoksza, D. Peptide-Binding site prediction from protein structure via points on the solvent accessible surface. In Proceedings of the 2018 ACM International Conference on Bioinformatics, Computational Biology, and Health Informatics. **2018**, 645, 645-650.
31. Ranjbar, A.; Jamshidi, M.; Torabi, S. Molecular modelling of the antiviral action of Resveratrol derivatives against the activity of two novel SARS CoV-2 and 2019-nCoV receptors. *Eur. Rev. Med. Pharmacol. Sci.* **2020**, *24*, 7834-7844.

32. van Brummelen, R.; van Brummelen, A.C. The potential role of resveratrol as supportive antiviral in treating conditions such as COVID-19 – A formulator's perspective. *Biomed. Pharmacother.* **2022**, *148*, 112767.
33. Hasan, A.H.; Yusof, F.S.; Kamarudin, N.A.; Murugesan, S.; Shakya, S.; Jamalis, J. Synthesis, anti-acetylcholinesterase evaluation, molecular docking and molecular dynamics simulation of novel psoralen derivatives. *Curr. Org. Synth.* **2024**, *21*, 61-77.
34. Al-Hazmi, G.H.; Ibrahim, A.A.; Refat, M.S.; Adam, F.A.; Allam, A.; Shakya, S.; Alsuhaibani, A.M. Intermolecular charge-transfer complexes between chlorothiazide antihypertensive drug against iodine sigma and picric acid pi acceptors: DFT and molecular docking interaction study with Covid-19 protease. *J. Indian Chem. Soc.* **2022**, *99*, 100605.
35. Alkathiri, A.A.; Atta, A.A.; Refat, M.S.; Altalhi, T.A.; Shakya, S.; Alswat, M.; Adam, A.M.A.; Mersal, G.A.; Hassanien, A.M. Preparation, spectroscopic, cyclic voltammetry and DFT/TD-DFT studies on fluorescein charge transfer complex for photonic applications. *Bull. Chem. Soc. Ethiop.* **2023**, *37*, 515-532.
36. Alsuhaibani, A.M.; Refat, M.S.; Adam, A.M.A.; Kobeasy, M.I.; Kumar, D.N.; Shakya, S.; Synthesis, spectroscopic characterizations and DFT studies on the metal complexes of azathioprine immunosuppressive drug. *Bull. Chem. Soc. Ethiop.* **2022**, *36*, 73-84.